33RD CONGRESS
OF THE INTERNATIONAL COUNCIL
OF THE AERONAUTICAL SCIENCES
STOCKHOLM, SWEDEN, 4–9 SEPTEMBER, 2022

ICAS
2022
SWEDEN

UNSTEADY SIMULATIONS OF MASSIVELY SEPARATED FLOW AROUND NACA0021 AIRFOIL USING A TRANSITIONAL IDDES MODEL

Yue Wang[1*], Shiqiang Zhang[2*], Wenping Song[3], Zhonghua Han [4]

[1] National Key Laboratory of Aerodynamic Design and Research, School of Aeronautics, Northwestern Polytechnical University, Xi'an, 710072, China
[2] Jilin Chongtong Chengfei New Material Co.,LTD. , Chongqing, 401336, China
[*] These authors contribute equally to this paper.

Abstract

A blended IDDES and correlation-based transition model, named as the γ-IDDES model, has been newly added in OpenFOAM v2106 to simulate the massively separated flow around NACA0021 airfoil at the angles of attack (AoAs) from 30° to 90°. Compared to the fully turbulent SST-IDDES model and the γ-SST RANS model, the γ-IDDES model can give the best predictions on the lift and drag coefficients at all the AoAs. At the AoAs of 30° and 40°, both the γ-IDDES model and the γ-SST RANS model can perform a little better than the SST-IDDES model on the predictions of lift and drag coefficients. This hints that the boundary layer transition may play a notable role in the simulation of massively separated flow by the subsequent flow analysis. When the AoAs are larger than 50°, both the γ-IDDES model and the SST-IDDES model can give accurate predictions on the lift and drag coefficients. In contrast, the γ-SST RANS model fails in the prediction of lift and drag coefficients. This illustrates that the capacity of capturing the flow structures is still essential in the simulation of massively separated flow.

Keywords: Transitional IDDES model, Hybrid RANS/LES, Correlation-based transition model

1. Introduction

Accurate modeling and simulation of massively separated flow around airfoils is still a challenging CFD problem of significant importance for the aerospace industry and wind energy. Boundary layer transition at the leading edge of airfoils may play an important role on the transformation from attached flow to massively separated flow around airfoils. Unfortunately, both the boundary layer transition and the massively separated flow are challenges in the modern CFD modeling.

At present, direct numerical simulation (DNS) and large eddy simulation (LES) can accurately simulate both the boundary layer transition and the massively separated flow. However, both of them require excessively large number of grid points and huge computational resources for engineering applications at high Reynolds numbers. In order to resolve turbulent flows in engineering applications at an affordable computational expense, hybrid RANS/LES approaches were developed to solve the boundary layer with Reynolds averaged Navier-Stokes (RANS) simulation and apply an LES treatment in the separated regions. However, the former hybrid RANS/LES methods were coupled with fully turbulent RANS models. They failed in the prediction of boundary layer transition [1].

In the past couple of years, a number of transition RANS models have been proposed, such as the e^N method[2-4] based on linear stability theory, low Reynolds number turbulent models[5], the laminar fluctuation energy method[6], the local-correlation-based transition models (LCTM)[7-10], the newly development methods based on Dynamic Mode Decomposition[11-12], and some other new physics-based transition models[13-17]. These transition RANS models can give good predictions of the boundary layer transition with high efficiency. However, these transition RANS models failed to predict the massively separated flow at present.

Considering the advantages and disadvantages of transition RANS models and hybrid RANS/LES

methods, it is logical to couple transition RANS models in the hybrid RANS/LES methods instead of fully turbulent models. Sorensen et al.[18] coupled the γ-Re$_\theta$-SST RANS model and the DES (detached-eddy simulation) model to predict the drag crisis of a circular cylinder. They discovered that this kind of DES-γ-Re$_\theta$ model performed better than the fully turbulent DES model. Kwon and You[19] proposed a blending function to smoothly combine the γ-Re$_\theta$-SST RANS model with the SAS (scale adaptive simulation) or DES model to simulate the supercritical flow past a circular cylinder. Qiao et al.[20] applied the γ-Re$_\theta$-DDES (delayed detached-eddy simulation) model to simulate the attached flow past a flat plane. Yi et al.[21] adopted a γ-Re$_\theta$-IDDES (improved delayed detached-eddy simulation) model to predict the roughness-induced transition at hypersonic speed. Xiao et al.[22] coupled the k-ω-γ RANS model with the DDES model to simulate the transition and massively separated flow past the Orion capsule at hypersonic speed.

In this paper, a blended IDDES (improved delayed detached-eddy simulation) and correlation-based transition model is newly added in OpenFOAM v2106 to simulate the massively separated flow around NACA0021 airfoil. The one equation local correlation based transition model of Menter et al.[23] (γ-transition model, Flow Turbulence Combustion, vol. 95, no. 4, pp. 583–619, 2015) is employed to simulate the boundary layer transition instead of the original fully turbulent kOmegaSST model. Hence, the newly added transitional IDDES model can be termed as the γ-IDDES model. In order to have a fully study on the accuracy of γ-IDDES model, comparisons are taken with the experimental data and the simulation results of the original fully turbulent SST-IDDES model and the γ-SST RANS model at large range angles of attack (AoAs).

2. Numerical Methodology

2.1 RhoPimpleFoam solver in OpenFOAM

All the simulations are carried out using the rhoPimpleFoam solver within the open source software OpenFOAM v2106. The rhoPimpleFoam solver employs the finite volume method for numerical representation of the compressible three-dimensional Navier-Stokes equations. As suggested by Robertson [24], a standard three-level 2nd order backward difference is used for the time marching scheme. For spatial discretization, the 2nd order cell-based scalar limiting central difference is used for the gradient term; the 2nd order bounded central difference for the divergence scheme and the 2nd order limited deferred correction scheme for the Laplacian scheme. In order to speed the calculations, message passing interface (MPI) is used for parallel computing.

2.2 A blended IDDES and correlation-based transition model

The coupling model is constructed based on the improved delayed detached-eddy simulation (IDDES) model[25] and the γ-transition model[23]. Both the IDDES model and the γ-transition model are built upon the shear-stress transport (SST) turbulence model [26]. The IDDES method is formulated by substituting the SST RANS length scale with the IDDES length scale in the destruction term of the turbulence kinetic energy (TKE) transport equation while keep the ω equation unmodified. The TKE equation of the SST-IDDES can be written as

$$\frac{\partial(\rho k)}{\partial t} + \frac{\partial(\rho u_j k)}{\partial x_j} = P_k - \frac{\rho k^{\frac{3}{2}}}{l_{IDDES}} + \frac{\partial}{\partial x_j}\left[(\mu + \sigma_k \mu_t)\frac{\partial k}{\partial x_j}\right] \tag{1}$$

where *k* is the modeled TEK. The IDDES length scale l_{IDDES} is defined as

$$l_{IDDES} = \tilde{f}_d(1 + f_e)l_{RANS} + (1 - \tilde{f}_d)l_{LES} \tag{2}$$

$$\tilde{f}_d = \max\{(1 - f_{dt}), f_b\} \tag{3}$$

$$f_{dt} = 1 - \tanh[(C_{dt1} \cdot r_{dt})^{C\_dt2}] \tag{4}$$

$$r_{dt} = \frac{\nu_t}{\kappa^2 d_w^2 \sqrt{0.5(S^2 + \Omega^2)}} \tag{5}$$

$$f_b = \min\{2\exp(-9\alpha^2), 1.0\} \tag{6}$$

$$\alpha = 0.25 - d_w/h_{max} \tag{7}$$

$$f_e = f_{e2} \cdot \max((f_{e1} - 1.0), 0.0) \tag{8}$$

$$f_{e1} = \begin{cases} 2 \cdot \exp(-11.09 \cdot \alpha^2), \alpha \geq 0 \\ 2 \cdot \exp(-9.0 \cdot \alpha^2), \alpha < 0 \end{cases} \tag{9}$$

$$f_{e2} = 1.0 - \max(f_t, f_l) \tag{10}$$

$$f_t = \tanh((C_t^2 \cdot r_{dt})^3) \tag{11}$$

$$f_l = \tanh((C_l^2 \cdot r_{dl})^{10}) \tag{12}$$

$$r_{dl} = \frac{\nu}{\kappa^2 d_w^2 \sqrt{0.5(S^2 + \Omega^2)}} \tag{13}$$

where l_{RANS} and l_{LES} are the turbulent length scale of the RANS and the subgrid length scale of the LES, respectively. More parameters can be accessed in the Ref. [25]. The model constants are:

$$C_{dt1} = 20, \ C_{dt2} = 3, \ C_l = 5.0, \ C_t = 1.87 \tag{14}$$

In the γ-IDDES model, the transport equation for the intermittency γ has been introduced as

$$\frac{\partial(\rho\gamma)}{\partial t} + \frac{\partial(\rho u_j k)}{\partial x_j} = P_\gamma - E_\gamma + \frac{\partial}{\partial x_j}\left[\left(\mu + \frac{\mu_t}{\sigma_\gamma}\right)\frac{\partial\gamma}{\partial x_j}\right] \tag{15}$$

The transition source term P_γ is defined as:

$$P_\gamma = F_{length}\rho S\gamma(1 - \gamma)F_{onset} \tag{16}$$

The magnitude of this source term is controlled by the transition length function, F_{length}, which used to be a correlation, but has been changed to a constant value 100. The formulation of the function F_{onset}, which is used to trigger the intermittency production. It contains the ratio of the local vorticity Reynolds number Re_V to the critical Reynolds number $Re_{\theta c}$. The critical Reynolds number $Re_{\theta c}$ is calculated algebraically using k and other local variables. As a result, the transition onset is controlled by the following functions:

$$F_{onset1} = \frac{Re_V}{2.2Re_{\theta c}}, F_{onset2} = \min(F_{onset1}, 2.0),$$

$$F_{onset3} = \max(1 - \left(\frac{R_T}{3.5}\right)^3, 0), F_{onset} = \max(F_{onset2} - F_{onset3}, 0) \tag{17}$$

The destruction/relaminarization source term E_γ is defined as:

$$E_\gamma = c_{a2}\rho\Omega\gamma F_{turb}(c_{e2}\gamma - 1) \tag{18}$$

where

$$F_{turb} = e^{-(\frac{R_T}{2})^4}, \quad c_{a2} = 0.06, \quad c_{e2} = 50 \tag{19}$$

The coupling between the IDDES model and the correlation-based transition model is accomplished mainly by modifying the production term in the TKE equation (1) of the IDDES model. The modified production term is

$$\tilde{P}_k = \gamma P_k + P_k^{lim} \tag{20}$$

An additional production term P_k^{lim} has been introduced in the modified production term to ensure proper generation of k at transition points for arbitrary low *Tu* levels. The expression for the P_k^{lim} is:

$$P_k^{lim} = 5C_k \max(\gamma - 0.2, 0)(1 - \gamma)F_{on}^{lim}\max(3C_{SEP}\mu - \mu_t, 0)S\Omega \tag{21}$$

$$F_{on}^{lim} = \min(\max\left(\frac{Re_V}{2.2 \cdot Re_{\theta c}^{lim}} - 1, 0\right), 3) \tag{22}$$

$$F_{\theta c}^{lim} = 1100 \tag{23}$$

Many parameters succeed from the γ-transition model [23].

3. Case Description and Grid Generation

3.1 Case Description

Unsteady simulations are carried on the massively separated flow around NACA0021 at large range angles of attack from 30° to 90°. The experimental study was conducted by Swalwell et al.[27] which involved an informative database of time-averaged quantities as well as instantaneous flow characteristics. Some key experimental flow parameters are presented in Table 1. They are strictly satisfied in the numerical simulations.

For all unsteady simulations, a non-dimensional time step *dt = Δt×U∞/c = 0.04* is used, where *Δt* is the physical time step, *U∞* is the freestream velocity and *c* is the length of chord. It has been approved that such time-step is fine enough to capture the transition flows [28-30]. Each simulation

has been run with *50xc/U∞* in advance to eliminate the effect of initial conditions and with subsequent *1200xc/U∞* for data collection and averaging analysis for the mean flow field.

Table 1 – Flow parameters from the experiment

Parameter	Notation	Value
Reynolds number	*Re*	2.7×10^{-5}
Chord length	*c*	0.125 m
Angle of attack	*α*	30° to 90°, every 10°

(a) "O-grid"	(b) "C-grid"
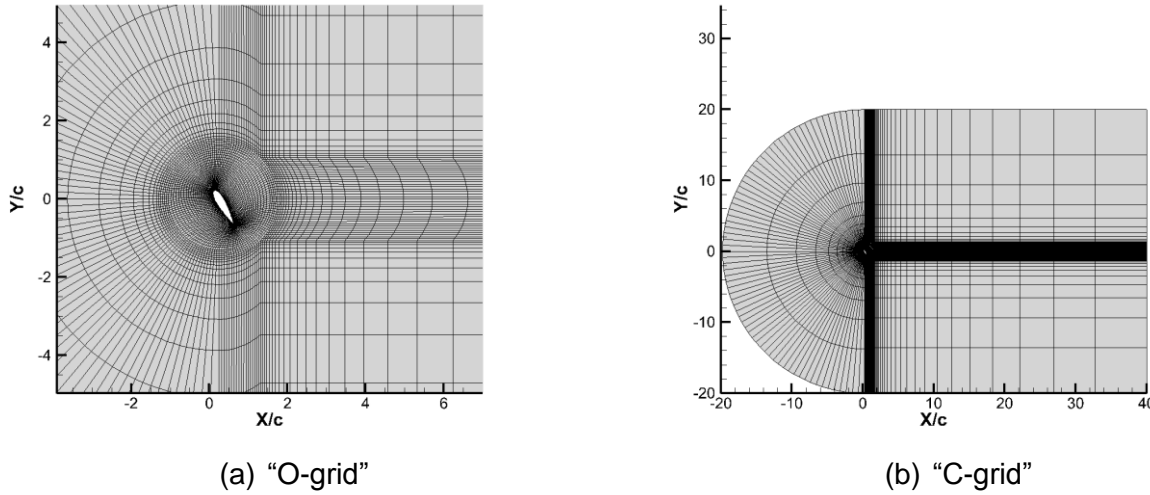
Figure 1 – "CO-grid" mesh topology (AoA = 60°).

3.2 Grid Generation and Boundary Conditions

The mesh topology in the computational domain is shown in Figure 1, which can be described as "CO-grid". A small O-grid is generated with growing boundary layers around the NACA0021 airfoil that can be seen in Figure 1a. The diameter of this O-grid is three times of the chord (c) of NACA0021 airfoil. The O-grid can be rotated as the AoA change. For example, the AoA is 60° in Figure 1. The C-grid is on the outside of the O-grid and extended to 20c in the upstream direction and 40c in the downstream direction. Such a CO-grid can minimize the skewness of a near-wall mesh, avoid high aspect ratio of grids in the far wake and form a fine enough mesh to solve the unsteady wake flow. In the span-wise direction, CO-grid is extruded with one chord (c) length by 40 layers. The boundary condition for the NACA0021 airfoil is no-slip adiabatic wall. The far-field boundary normal the wake flow is considered as outlet flow boundary condition with no back flow. The other far-field boundaries are considered as velocity inlet flow. The front and back boundaries are set as the periodic boundary condition for the 3D simulations.

4. Results and Discussion

4.1 Grid Sensitivity Study

Grid sensitivity study has been done at the AoA of 60° via γ-IDDES simulations with three grids. Details of the three grids are list in Table 2. Three grid resolution levels are elaborately designed with an approximate 2 times increases of total cells from the coarse grid to the fine grid. There are total 242 720, 477 760 and 952 000 grid cells respectively. The wrap-around points on the airfoil are 104, 144 and 200, respectively. The spanwise layers are kept as the same with 40 layers. The maximum yplus is controlled fewer than 2 to ensure the enough grid resolution in the boundary layer. In Figure 2, the pressure coefficient (Cp) distributions on the surface of the airfoil show a good convergence with the grid refinement and have a good comparison to the experimental data. The *Cp* curves of the medium and fine meshes are almost coincide with each other. Considering the requirement of huge computational resources, the medium mesh is selected for the simulations of other AoAs.

Table 2 – Details of the grids in the grid sensitivity study

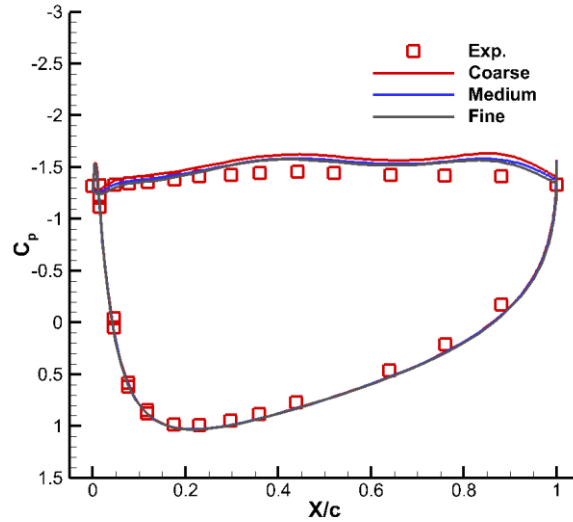| Grid level	Total cells	Wrap-around points	Spanwise layers	Max. yplus
Coarse	242,720	104	40	1.90
Medium	477,760	144	40	1.37
Fine	952,000	200	40	0.97

Figure 2 – Grid sensitivity study (AoA = 60°).

4.2 Overall comparison

The target of this study is to verify the capability of γ-IDDES model in the simulations of massively separated flow around NACA0021 airfoil. The AoAs range from 30° to 90° at every 10°. In order to have a comprehensive understanding on the performance of γ-IDDES model, both the original fully turbulent SST-IDDES model and the γ-SST RANS model are adopted for a comparison.

Figure 1 shows the overall comparison of lift and drag coefficients among simulation results and experimental data [27]. The γ-IDDES simulations show the best predictions on the lift and drag coefficients among the three models at all the AoAs from 30° to 90°. The fully turbulent SST-IDDES model has performed not badly if it is examined with only itself compared to the experimental data. When the AoAs are large the 50°, the predicted curves using the SST-IDDES model almost coincide with the predicted curves using the γ-IDDES model on the lift and drag coefficients. However, at the AoAs of 30° and 40°, the SST-IDDES model gives the worst predictions among the three models. In contrast, the γ-SST RANS model can give predictions as good as the γ-IDDES model at the AoAs of 30° and 40°. This hints that the correlation-based transition model may play a notable role on the simulations at the AoAs of 30° and 40°. However, the γ-SST RANS model performs badly when the AoAs are large than 50°. The lift coefficients predicted by the γ-SST RANS model show large deviations from the experimental data when the AoAs are large than 50°. The absolute deviations increase at the AoAs from 50° to 70°, then decrease from 70° to 90°. The drag coefficients predicted by the γ-SST RANS model have larger deviations as the AoAs increasing form 50° to 90°. This illustrates that the γ-SST RANS model cannot capture the large separations on these large AoAs. In an overall comparison, the γ-IDDES model can take the advantage of transition modeling from the γ-SST RANS model and the advantage of separation modeling from the SST-IDDES model. As a result, the γ-IDDES model can give the most accurate prediction among the three models on the lift and drag coefficients on the massively separated flow around NACA0021 airfoil at the AoAs from 30° to 90°.
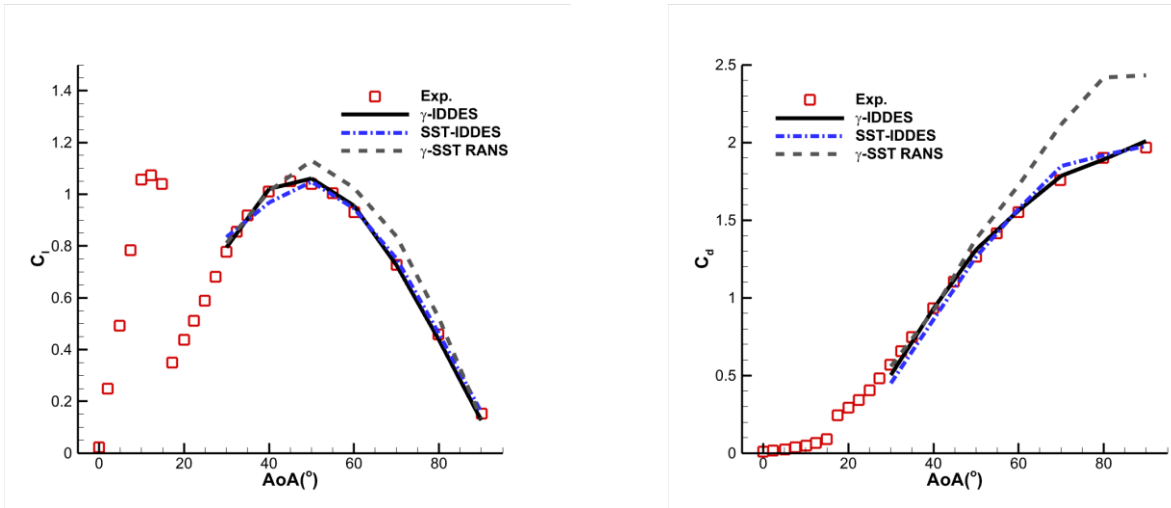
(a) Lift coefficient   (b) Drag coefficient

Figure 3 – Overall comparison of lift and drag coefficients among simulation results and experimental data [27].
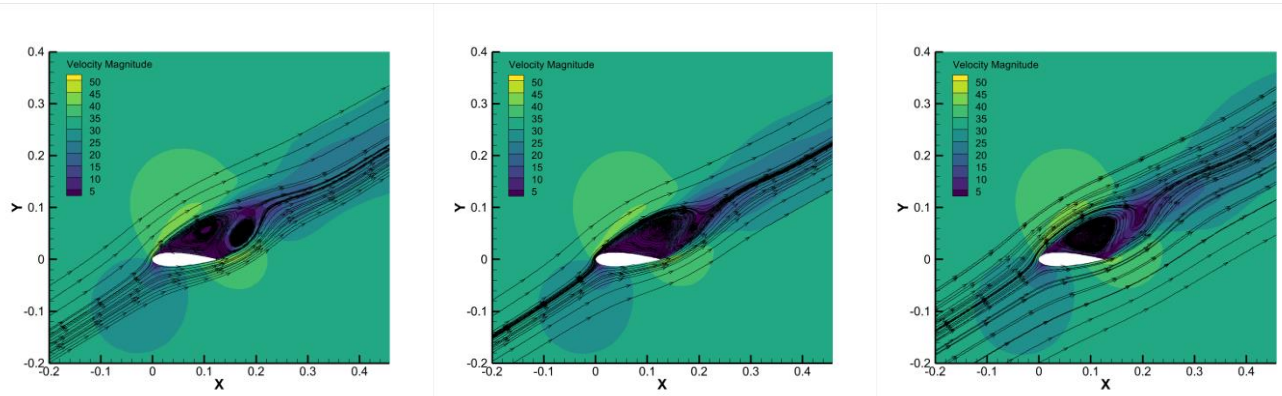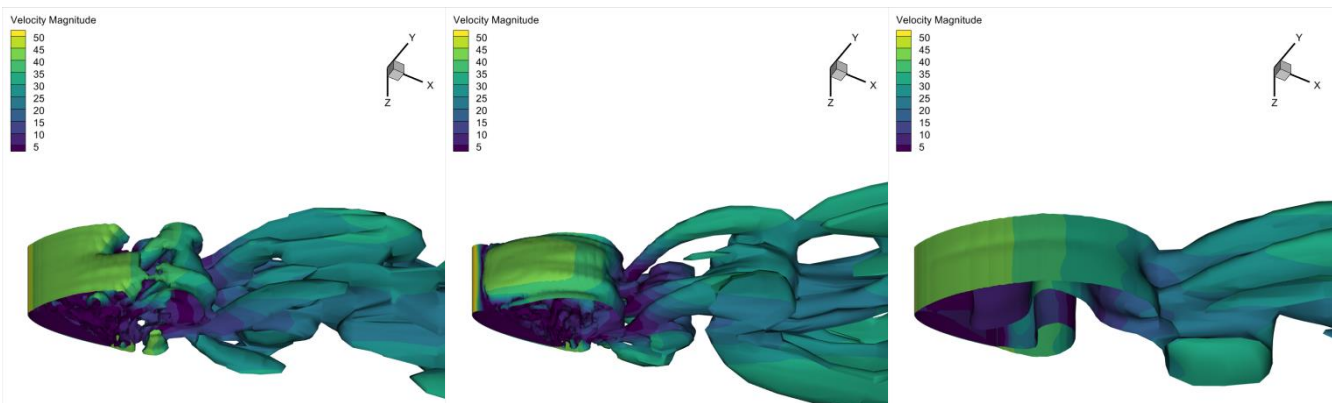

(a) γ-IDDES   (b) SST-IDDES   (c) γ-SST RANS

Figure 4 – Comparison of mean flow field by velocity magnitude and streamlines (AoA = 30°)

(a) γ-IDDES   (b) SST-IDDES   (c) γ-SST RANS

Figure 5 – Comparison of transient flow structures by Q criterion (AoA = 30°, Q = 100)

4.3 Flow analysis and comparison

Since the γ-IDDES model can take the advantages from the γ-SST RANS model and the SST-IDDES model, give the most accurate prediction of the lift and drag coefficients, it is very interesting to make a deep study with the flow analysis and comparison among simulations with different models. In this section, three AoAs are selected for the flow analysis and comparison.

When the AoA is 30°, the γ-IDDES model and the γ-SST RANS model can give a little better prediction than the SST-IDDES model which has been found in Figure 3. Figure 4 shows the comparison of mean flow field by velocity magnitude and streamlines at the AoA of 30°. Since the

flow has been already massively separated at the AoA of 30°, all the mean flow fields show large recirculation regions in the wake flow simulations using the three models. The difference is that there are two vortex cores found in the γ-IDDES simulations. In contrast, only one vortex core can be found completely in the SST-IDDES model and the γ-SST RANS model. It is hard to say which flow pattern is correct without the detailed flow observation from experiments. The deviations of lift and drag coefficients are not large in general between the experimental data and the simulation results.

Figure 5 shows the comparison of transient flow structures by Q criterion at the AoA of 30°. The value of Q criterion is 100. From the Figure 5, more flow structures can be found in the γ-IDDES and SST-IDDES simulations. In contrast, the γ-SST RANS model can only capture the vortexes at the largest scale. This difference is reasonable since the IDDES-type simulations employ the LES treatment outside of the boundary layer. There is a notable difference on the flow structures at the leading edge. The γ-IDDES and γ-SST RANS simulations own a similar shear flow structure at the beginning of the leading edge. However, there is a delay and fracture of the shear flow at the leading edge in the SST-IDDES simulation. The fracture makes the low velocity flow structures shown in the view of Figure 5. This difference may be caused by the transition model. The transition model may generate smooth structures connecting the shear flow. In contrast, the fully turbulent RANS model may cause the interruption on the shear flow and generate the fracture on the shear flow. This small difference at the leading edge may be used to explain why the γ-IDDES model and the γ-SST RANS model can give better predictions than the SST-IDDES model.
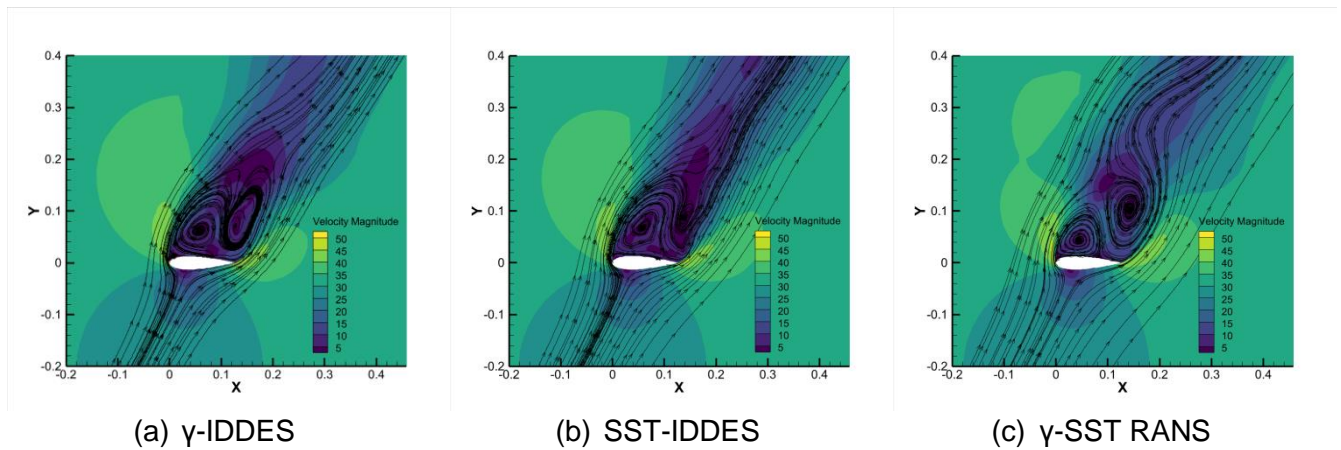

(a) γ-IDDES   (b) SST-IDDES   (c) γ-SST RANS

Figure 6 – Comparison of mean flow field by velocity magnitude and streamlines (AoA = 60°)
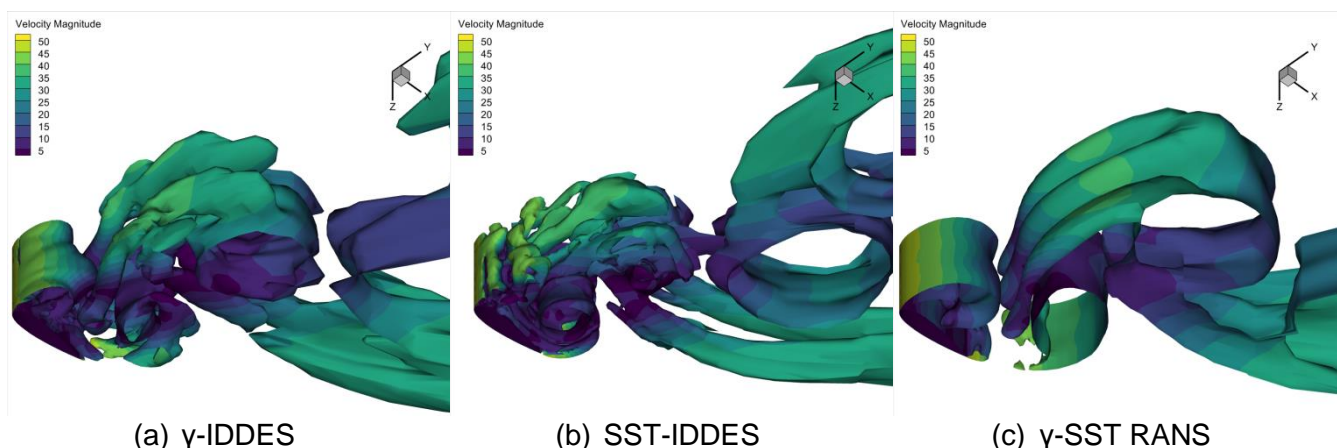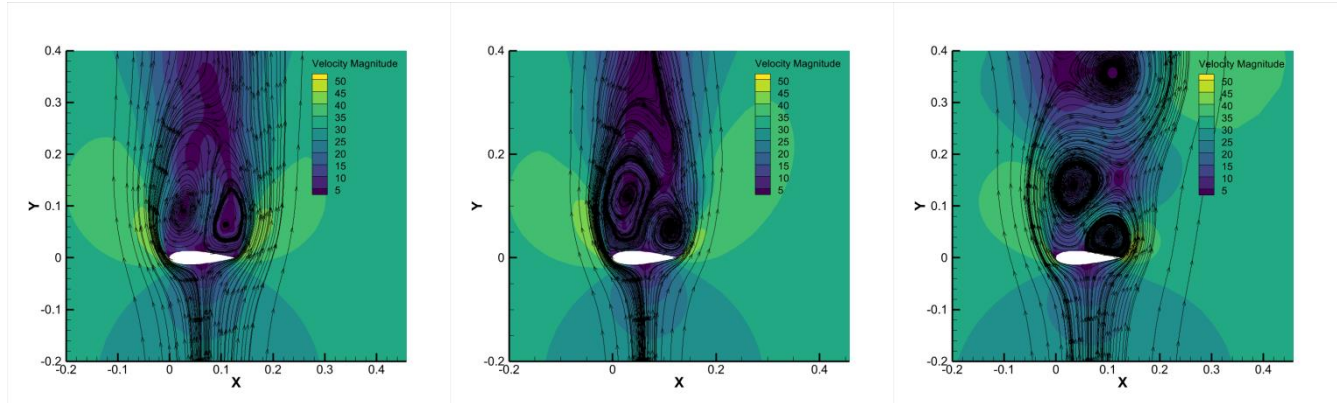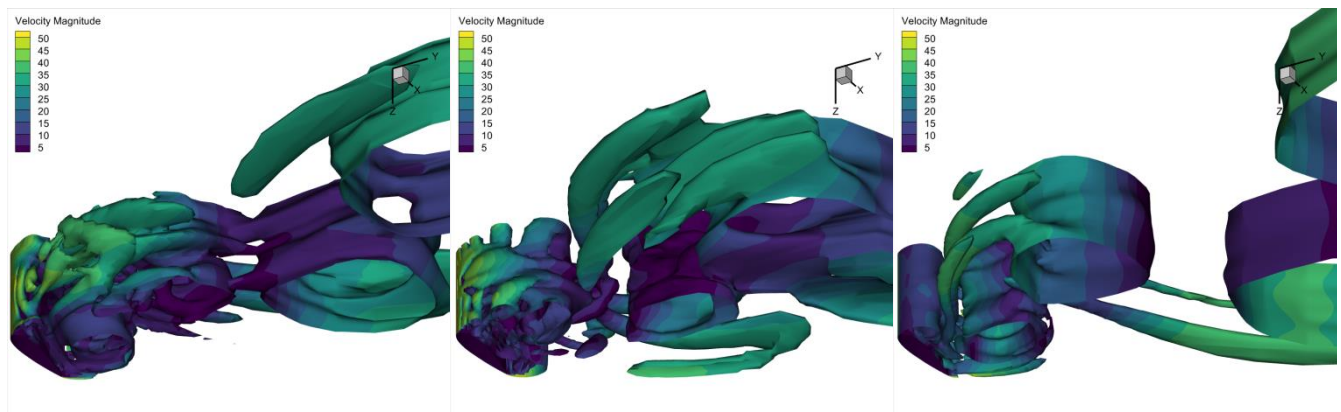

(a) γ-IDDES   (b) SST-IDDES   (c) γ-SST RANS

Figure 7 – Comparison of transient flow structures by Q criterion (AoA = 60°, Q = 100)

When the AoA equals 60°, both the γ-IDDES model and the SST-IDDES model can give accurate predictions on the lift and drag coefficients. In contrast, there are large deviations between the γ-SST RANS simulation results and the experimental data. The RANS-type model cannot capture the correct flow structures at the AoA of 60°. This conclusion has been recognized by many researchers [28-34]. However, before this study, no simulation has been done using the γ-IDDES model and the γ-SST RANS model. Figure 6 shows the comparison of mean flow field among the

three models used in this study. There are two vortex cores which can be found in the mean flow field of all the three simulations using different models. However, the distribution of the two vortexes looks similar between the two IDDES-type simulations. The vortex close to the leading edge is larger than the vortex close to the trailing edge. In contrast, in the γ-SST RANS simulation, the vortex close to the leading edge is smaller than the vortex close to the trailing edge. That is the main difference of the mean flow field between the γ-SST RANS simulation and the two IDDES-type simulations.

| (a) γ-IDDES | (b) SST-IDDES | (c) γ-SST RANS |

Figure 8 – Comparison of mean flow field by velocity magnitude and streamlines (AoA = 90°)

| (a) γ-IDDES | (b) SST-IDDES | (c) γ-SST RANS |

Figure 9 – Comparison of transient flow structures by Q criterion (AoA = 90°, Q = 100)

Figure 10 shows the comparison of transient flow structures among the simulations using three different models at the AoA of 60°. Generally, the transient flow structures of γ-SST RANS simulation still show a big difference from the two IDDES-type simulations. Only the flow structures at the largest scale can be simulated in the γ-SST RANS simulation. The IDDES-type simulations can capture smaller flow structures compared to the γ-SST RANS simulation. There is a difference found between the γ-IDDES simulation and the SST-IDDES simulation. In the SST-IDDES simulation, there is no complete shear layer found close to the leading edge. The shear layer is broken into strips. Fractures are found in the transient flow structures in the SST-IDDES simulation. In contrast, the shear layer is relative complete in the γ-IDDES simulation. This flow structure looks similar to the shear layer found in the γ-SST RANS simulation. This may be still decided by the transition model in both the γ-IDDES simulation and the γ-SST RANS simulation. However, this relative complete shear layer is not the dominant flow structure in the prediction of lift and drag coefficients. The accurate simulation of the flow structures in the recirculation region can decide the prediction of the lift and drag coefficients. That is the reason why the γ-SST RANS simulation gives poor predictions on both lift and drag coefficients at the AoA of 60°.

When the AoA equals 90°, huge recirculation regions can be found in the mean flow field of the two IDDES-type simulations (Figure 11 (a) and (b)). In contrast, the mean flow field of the γ-SST RANS simulation (Figure 12 (c)) is quite different from the two IDDES-type simulations. There is no huge recirculation region which can cover the whole top surface of the NACA0021 airfoil. There is only

one vortex close the trailing edge and vortexes in the wake flow. In such a mean flow field, the drag coefficient predicted by the γ-SST RANS simulation is very poor with a large deviation compared to the experimental data at the AoA of 90°. In contrast, both the γ-IDDES simulation and the SST-IDDES simulation can give accurate predictions on both the lift and drag coefficients. This illustrates that the mean flow field predicted by the two IDDES-type simulations may be more reasonable than the γ-SST RANS simulation.

Figure 13 shows the comparison of transient flow structures among the three different models at the AoA of 90°. The transient flow structures are similar between the two IDDES-type simulations. There are recirculation regions with small flow structures in the wake flow close to the airfoil. Beyond of the recirculation regions, the transient vortexes are generated one by one as the flow goes to the far field. In contrast, there is no recirculation region in the transient flow structure of the γ-SST RANS simulation. Without the recirculation region, it seems that the γ-SST RANS simulation cannot get the correct prediction on the drag coefficient at the AoA of 90°.

5. Conclusions

In this study, a blended IDDES and correlation-based transition model, named as the γ-IDDES model, has been newly added in OpenFOAM v2106 to simulate the massively separated flow around NACA0021 airfoil at the AoAs form 30° to 90°. The simulation results using this γ-IDDES model have been compared with the experimental data and unsteady simulation results using another two different models. One is the fully turbulent SST-IDDES model, the other one is the γ-SST RANS model.

A grid sensitivity study has been done by three different grids with the γ-IDDES simulation. The *Cp* distributions show a good convergence with the grid refinement and have a good comparison to the experiment data.

Compared to the fully turbulent SST-IDDES model and the γ-SST RANS model, the γ-IDDES model can give the best predictions on the lift and drag coefficients at all the AoAs from 30° to 90°. At the AoAs of 30° and 40°, both the γ-IDDES model and the γ-SST RANS model can perform a little better than the SST-IDDES model on the predictions of lift and drag coefficients. This phenomenon may be caused by the use of transition model due to flow structure analysis. This hints that the boundary layer transition may play a notable role in the simulation of massively separated flow by the subsequent flow analysis.

When the AoAs are larger than 50°, both the γ-IDDES model and the SST-IDDES model can give accurate predictions on the lift and drag coefficients. In contrast, the γ-SST RANS model fails in the predictions of lift and drag coefficients. This illustrates that the capacity of capturing the flow structures is still essential in the simulation of massively separated flow.

6. Acknowledgments

7. Contact Author Email Address

Mailto: yuewang@nwpu.edu.cn

8. Copyright Statement

References

[1] Frohlich J, Von Terzi D. Hybrid LES/RANS methods for the simulation of turbulent flows. *Prog. Aerosp. Sci.*, Vol.44, No.5, pp 349-377, 2008.

[2] Drela M, Giles M B. Viscous-inviscid analysis of transonic and low Reynolds number airfoils. *AIAA J.*, Vol.25, No.10, pp 1347-1355, 1987.

[3] Shi Y Y, Yang T H, Bai J Q, et al. Research of transition criterion for semi-empirical prediction method at specified transonic regime. *Aerosp. Sci. Technol.,* Vol.88, pp 95-109, 2019.

[4] Halila G L O, Chen G D, Shi Y Y, et al. High-Reynolds number transition flow simulation via parabolized stability equations with an adaptive RANS solver. *Aerosp. Sci. Technol.,* Vol. 91, pp 321-336, 2019.

[5] Wilcox D A. Simulation of transition with a two-equation turbulence model. *AIAA J.*, Vol. 32, No. 2, pp 247-255, 1994.

[6] Liu Z J, Zhao Y T, Chen S S, et al. Predicting distributed roughness induced transition with a four-equation laminar kinetic energy transition model. *Aerosp. Sci. Technol.* Vol. 99, 105736, 2020.

[7] Menter F R, Langtry R B, Likki S R, et al. A correlation based transition model using local variables part I –model formulation. *J. Turbomach*, Vol. 128, No. 3, pp 413-422, 2006.

[8] Menter F R, Langtry R B, Volker S. Transition modeling for general purpose FD codes. *Flow Turbul. Combust.*, Vol. 77, pp 277-303, 2006.

[9] Langtry R B, Menter F R. Correlation-based transition modeling for unstructured parallelized computational fluid dynamics codes. *AIAA J.,* Vol. 47, No. 12, pp 2894-2906, 2009.

[10] Liu K, Wang Y, Song W P, et al. A two-equation local-correlation-based laminar-turbulent transition modeling scheme for external aerodynamics. *Aerosp. Sci. Technol.,* Vol. 106, 106128, 2020.

[11] Wu M M, Han Z H, Nie H, et al. A transition prediction method for flow over airfoils based on high-order dynamic mode decomposition. *Chin. J. Aeronaut.,* Vol. 32, No.11, 2408-2421, 2019.

[12] Chainche S L, Han Z H, Ferrer E. Alternative method to study cross-flow instabilities based on high order dynamic mode decomposition. *Phys. Fluids*, Vol. 31, No. 9, 094101, 2019.

[13] Vizinho R, Morgado J, Pascoa J, et al. Analysis of transition flow in 3D geometries using a novel phenomenological model. *Aerosp. Sci. Technol.,* Vol 45, pp 431-441, 2015.

[14] Xu J K, Bai J Q, Qiao L, et al. Development of a computational fluid dynamics compatible mathematical model for boundary layer transition flows in low-disturbance environment. *Aerosp. Sci. Technol.,* Vol. 86, 487-496, 2019.

[15] Wang L, Fu S. Development of an intermittency equation for the modeling of the supersonic/hypersonic boundary layer flow transition. *Flow Turbul. Combust.*, Vol. 87, 165-187, 2011.

[16] Xu J K, Xu D, Zhang Y, et al. Capturing transition with flow-structure-adaptive KDO RANS model. *Aerosp. Sci. Technol.*, Vol. 85, 150-157, 2019.

[17] Xiao M J, She Z S. Symmetry-based description of laminar-turbulent transition. *Sci. China, Phys. Mech. Astron.,* Vol. 62, No. 9, pp 1-7, 2019.

[18] Sorensen N N, Bechmann A, Zahle F. 3D CFD computations of transition flows using DES and a correlation based transition model. *Wind Energy,* Vol. 14, No. 1, pp 77-90, 2011.

[19] Kwon O J, You J Y. Blending of SAS and correlation-based transition models for flow simulation at supercritical Reynolds numbers. *Comput. Fluids,* Vol.80, pp 63-70, 2013.

[20] Qiao L, Bai J Q, Hua J, et al. Combination of DES and DDES with a correlation based transition model. *Appl. Mech. Mater,* Vol. 444, pp 374-379, 2014.

[21] Yi M R, Zhao H Y, Le J L, et al. γ-Re$_θ$ transition model based on IDDES frame. *Acta Aeronaut. Astronaut. Sin.,* Vol. 40, No. 8, 122726, 2019.

[22] Xiao Z X, Wang G X, Yang M C, et al. Numerical investigations of hypersonic transition and massive separation past Orion capsule by DDES-Tr. *Int. J. Heat Mass Transf.,* Vol. 137, pp 90-107, 2019.

[23] Menter F R, Smirnov P E, Liu T, et al. A one-equation local correlation-based transition model. *Flow Turbu. Combust*, Vol. 95, No.4, pp 583-619, 2015.

[24] Robertson E, Choudhury V, Bhushan S, et al. Validation of OpenFOAM numerical methods and turbulence models for incompressible bluff body flows. *Computers & Fluids*, Vol. 123, pp 122-145, 2015.

[25] Gritskevich M S, Garbaruk A V, Schütze J, et al. Development of DDES and IDDES Formulations for the k-ω Shear Stress Transport Model. *Flow Turbulence & Combustion,* Vol. 88, No.3, pp 431-449, 2012.

[26] Menter F R. Two equation eddy-viscosity turbulence models for engineering applications. *AIAA J.,* Vol. 32, No. 8, PP 1598-1605, 1994.

[27] Swalwell K E, Sheridan K E, Melbourne W H. Frequency analysis of surface pressures on an airfoil after stall. *In: 21st applied aerodynamics conference,* Orlando, 2003.

[28] Wang Y, Song B F, Song W P, et al. Partially-averaged Navier-Stokes simulations of unsteady flow around NACA0021 airfoil at 60° angle of attack. *AIAA AVIATION Forum applied aerodynamic*

conference, Atlanta, Georgia, 2018.

[29] Wang Y, Liu K, Song W P, et al. Scale adaptive simulations of unsteady flow around NACA0021 airfoil at 60° angle of attack. *AIAA Scitech Forum,* San Diego, California, 2019.

[30] Wang Y, Liu K, Han Z H. Detached eddy simulation on the flow around NACA0021 airfoil beyond stall using OpenFOAM. *Asia-Pacific International Symposium on Aerospace Technology*, Chendu, China, 2018.

[31] Akoury R E, Braza M, Hoarau Y, et al. Unsteady flow around a NACA0021 airfoil beyond stall at 60° angle of attack. *In: IUTAM symposium on unsteady separated flows and their control, IUTAM Bookseries 14,* 2019.

[32] Garbaruk A, Leicher S, Mockett C, et al. Evalution of time sample and span size effects in DES of nominally 2D airfoils beyond stall. *In: Peng S-H, Haase W (eds) Progress in hybrid RANS-LES modeling, pp 87-99, Springer,* Berlin, 2010.

[33] Zheng W L, Yan C, Liu H K, et al. Comparative assessment of SAS and DES turbulence modeling for massively separated flows. *Acta Mech. Sim.* Vol. 32, No. 1, pp 12-21, 2016.

[34] Zhang Y, Zhang L P, He X, et al. An improved second-order finite-volume algorithm for detached-eddy simulation based on hybrid grids. *Communications in computational physics,* Vol. 20, Issue 02, pp 459-485, 2016.